Microwave heating mechanism and self-healing performance of asphalt mixture with basalt and limestone aggregates

Wang, Fu; Zhu, Hongbin; Shu, Benan; Li, Yuanyuan; Gu, Dengjun; Gao, Yangming; Chen, Anqi; Feng, Jianlin; Wu, Shaopeng; More Authors

DOI
10.1016/j.conbuildmat.2022.127973

Publication date
2022

Document Version
Final published version

Published in
Construction and Building Materials

Construction and Building Materials 342 (2022) 127973

Contents lists available at ScienceDirect

Construction and Building Materials

journal homepage: www.elsevier.com/locate/conbuildmat

Microwave heating mechanism and self-healing performance of asphalt mixture with basalt and limestone aggregates

Fu Wang [a], Hongbin Zhu [a], Benan Shu [b], Yuanyuan Li [a,*], Dengjun Gu [a], Yangming Gao [c], Anqi Chen [d,*], Jianlin Feng [a], Shaopeng Wu [d], Quantao Liu [d], Chao Li [b]

[a] School of Civil Engineering and Architecture, Wuhan Institute of Technology, Wuhan 430074, China
[b] Foshan Transportation Science and Technology Co., Ltd, Foshan 528315, Guangdong, China
[c] Marie S. Curie Research Fellow Section of Pavement Engineering, Faculty of Civil Engineering & Geosciences, Delft University of Technology, Stevinweg 1, 2628 CN Delft, The Netherlands
[d] State Key Laboratory of Silicate Materials for Architectures, Wuhan University of Technology, Wuhan 430070, Hubei, China

ARTICLE INFO

Keywords:
Basalt
Aggregates
Asphalt mixture
Microwave heating mechanism
Heating characteristics
Self-healing performance

ABSTRACT

Traditional asphalt mixtures can't absorb microwave energy efficiently, which limits the development of microwave heating technology in the field of road maintenance. Based on the microwave heating characteristics of basalt aggregates, the overall microwave self-healing rate of the asphalt mixture can be enhanced. The basalt was tested by XRF, XPS, XRD and electromagnetic parameters to reveal its microwave heating mechanism. Through the heating rate test, SCB test and fatigue test of asphalt mixture, its heating characteristics, flexural strength, fatigue resistance and self-healing performance were studied. The results showed that the excellent wave-absorbing properties of basalt are highly correlated with the elements of Si, Fe and Al. Its $Tan\delta_M$ was slightly larger than $Tan\delta_E$, which indicated that basalt can absorb microwave energy through dielectric loss and magnetic loss. The aggregate type and particle size both affected the microwave heating rate of the aggregates. After microwave heating, the flexural strength and fatigue resistance of asphalt mixture with basalt and limestone aggregates can recover at least 65% and 23% respectively.

1. Introduction

Asphalt pavement is a flexible pavement, which has low noise when interacting with tires and good durability and wear resistance. It has become one of the most common pavement types [1]. The asphalt pavement cracks, its durability will decline sharply, and the road needs to be maintained [2]. However, long-time road maintenance will lead to traffic congestion, reduced driving safety factors and high axle load pressure in non-maintenance sections [3,4]. It can be seen that the road performance and road maintenance of conventional asphalt pavement is facing severe challenges.

Asphalt pavement is paved with asphalt mixture composed of asphalt, mineral aggregates and filler [5], the service life of asphalt pavement is closely related to the mechanical strength and shape of aggregates [6]. Aggregates ensure the stable structural strength of the asphalt mixture [7], so there are higher requirements for aggregates in the design of asphalt pavement. Aggregates design includes two aspects. One is the selection of aggregate types. Granite, diabase and limestone are the most commonly used aggregate types for asphalt pavement [8,9]. The asphalt mixture pavement with granite aggregates has good high-temperature stability and good durability and wear resistance, but granite is acidic stone, and the water stability of granite asphalt mixture is poor [10]. Diabase has good thermal conductivity, and diabase asphalt pavement has good heating and deicing performance [11]. Basalt is also a commonly used aggregate type, which is generally used for high-grade pavement. The rutting resistance and skid resistance of basalt asphalt mixture pavement are better than that of limestone asphalt mixture pavement [12]. The adhesion between basalt and asphalt in a humid environment is better than that between limestone and asphalt [13], and the adhesion between basalt and asphalt is also better than that between granite and asphalt [14]. The other is the design of aggregate gradation, adhesion of aggregates and asphalt

* Corresponding authors.
E-mail addresses: wangfu@wit.edu.cn (F. Wang), 22004010115@stu.wit.edu.cn (H. Zhu), shuba@whut.edu.cn (B. Shu), Liyy@wit.edu.cn (Y. Li), 22004010016@stu.wit.edu.cn (D. Gu), Y.Gao-3@tudelft.nl (Y. Gao), anqi.chen@whut.edu.cn (A. Chen), 22004010110@stu.wit.edu.cn (J. Feng), wusp@whut.edu.cn (S. Wu), liuqt@whut.edu.cn (Q. Liu), lic@whut.edu.cn (C. Li).

https://doi.org/10.1016/j.conbuildmat.2022.127973
Received 30 January 2022; Received in revised form 25 May 2022; Accepted 25 May 2022
Available online 31 May 2022

affects the mechanical properties of asphalt mixture to a certain extent [15,16]. Panda [17] found that when the asphalt and aggregates were the same, the rutting resistance and deformation resistance of coarse-graded asphalt mixture is stronger than that of open-graded asphalt mixture. Guo [10] obtained from the comparative test that the water stability of asphalt mixture with coarse aggregates granite and fine aggregates limestone was significantly improved compared with granite asphalt mixture. The high-temperature stability of the asphalt mixture with basalt and limestone aggregates is better than that of the limestone asphalt mixture. Limestone makes up for the poor adhesion between basalt and asphalt to a certain extent [8]. The high-temperature stability and water stability of the asphalt mixture with diabase and limestone aggregates are improved compared with that of single aggregates (only diabase or limestone) asphalt mixture [9]. The adhesion of limestone to asphalt is better than that of basalt [8,14,18], and the mechanical strength of basalt is higher than that of limestone [19]. The combination of basalt and limestone can complement the two short plates so that the water stability and mechanical properties of the asphalt mixture can meet the standard and maintain a high level.

Since the proportion of aggregates in the asphalt mixture reaches more than 90% [5,20], From the aggregate aspect, the technical means that can not only quickly repair asphalt pavement diseases distresses, but also restore certain pavement performance can be studied. Asphalt mixture has self-healing performance [21–23], which is of great significance to its road performance and durability [1]. The self-healing performance of asphalt mixture is related to road maintenance to a certain extent [22]. However, due to the slow self-healing speed of conventional asphalt mixture, the generation rate of pavement cracks is much greater than its self-healing rate [5]. Accelerating the self-healing rate of asphalt mixture has become the research focus of road practitioners. The temperature of the asphalt mixture after heating determines its self-healing rate. The higher the temperature after heating, the faster the self-healing rate [2,24]. The self-healing rate can be improved by increasing the heating temperature of the asphalt mixture during the heating process. In recent years, many successful cases of using microwave heating to repair pavement distresses have attracted much attention in the road field. Martina [25] compared microwave heating with other existing methods to treat road distresses, and concluded that microwave heating had the advantages of depth, selectivity, high heating efficiency and uniformity. Microwave heating can induce asphalt mixture to accelerate self-healing. In the process of microwave heating, the microwave directly acts on the heated object without heat transfer process, so the energy utilization rate of microwave heating is high [26]. Materials that can be heated by microwave are called microwave absorbing materials, which can be divided into electric loss microwave absorbing materials and magnetic loss microwave absorbing materials [27]. For example, pyrolytic carbon black [28] and Si [29] are electric loss microwave absorbing materials, ferrite [30] and hot burned steel slag [2] are magnetic loss microwave absorbing materials. Therefore, the microwave heating technology is applied to the road field by researchers, and it is feasible to study the combination of aggregates and microwave heating technology.

The mechanism of microwave heating can be studied from the aspect of microwave parameters. The dielectric constant (ε) and magnetic permeability (μ) of the microwave absorbing material corresponds to the dielectric loss and magnetic loss respectively [31], and ε_r and μ_r represent the complex relative permittivity and complex relative permeability respectively, which are the main parameters to quantify the performance of electromagnetic waves [32]. The loss of microwaves by absorbing materials can be divided into dielectric loss and magnetic loss. The loss tangent represents the ability to lose microwaves, also known as the dissipation factor[33]. The imaginary part (ε“ and μ”) of the ε and μ characterize the lost energy, the real part (ε’ and μ’) of the ε and μ characterize the stored energy, dissipation factor (Tanδ) is the ratio of lost energy to stored energy [34]. tanδ_E and tanδ_M are respectively the dielectric loss angle tangent and the magnetic angle loss tangent, by comparing the dielectric loss tangent and magnetic loss tangent, the loss type of microwave absorbing material can be identified [35]. The real part values of dielectric constant and permeability represent the ability to store electric energy and magnetic energy respectively, and the imaginary part values represent the ability of dielectric loss and magnetic loss respectively [36]. The reflection loss (RL) characterizes the microwave absorption performance of the material [37,38]. Eqs. (1) and (2) are the calculation equations of RL.

$$Z_{in} = Z_0\sqrt{\frac{\mu_r}{\varepsilon_r}}\tanh\left(j\frac{2\pi fd}{c}\sqrt{\mu_r\varepsilon_r}\right) \tag{1}$$

$$RL = 20\lg\left|\frac{Z_{in}-Z_0}{Z_{in}+Z_0}\right| \tag{2}$$

In Eqs. (1) and (2), Z_{in} is the impedance of the absorbing layer (ohm), Z_0 is the impedance of free space (ohm), j is the imaginary unit, f is the electromagnetic wave frequency (GHz), d is the thickness of the absorbing layer (mm), and c is the speed of light (m/s).

Scholars used microwave heating technology to induce the self-healing of asphalt mixture with basalt and limestone aggregates, and all concluded that the self-healing performance of asphalt mixture with basalt and limestone aggregates was significantly improved [39–41]. Therefore, the combination of basalt aggregates and microwave heating technology has a good application prospect in the field of road maintenance. However, most of the research on basalt absorption of microwaves only stays at the phenomenon level of basalt absorbing microwaves and heating up, and rarely combines the chemical composition, elemental analysis and electromagnetic parameters of basalt to reveal its microwave absorption mechanism. The research on asphalt mixture with basalt and limestone aggregates focuses on the mechanical properties and self-healing properties, and rarely combines its heating characteristics and self-healing properties. The self-healing performance evaluation of asphalt mixture after microwave heating is only carried out by −10 °C semicircular bending (SCB) test, and there is basically no 25 °C fatigue test. It is even rarer to comprehensively evaluate the performance of asphalt mixture through the −10 °C SCB test and the 25 °C fatigue test. The less the number of healing cycles of the asphalt mixture, the less representative the self-healing rate data is.

The asphalt mixture with basalt and limestone aggregates is used to design the asphalt mixture with basalt and limestone aggregates, which is intended to enhance the microwave absorption performance of the asphalt mixture. The basalt aggregates in the asphalt mixture can absorb higher microwave energy under the action of microwave, to improve the overall self-healing performance of the asphalt mixture. It is proposed that under the maintenance technology of microwave technology, the relevant performance of asphalt pavement can be restored well. The chemical composition test, elemental analysis test, phase composition test and electromagnetic parameter test was carried out on the basalt, and the physicochemical and electromagnetic properties of the basalt were comprehensively analyzed to reveal its absorption mechanism. Microwave heating of aggregates and asphalt mixture was conducted to study the heating characteristics of aggregates and asphalt mixture. SCB test will be used to carry out fracture – healing – fracture on asphalt mixture, fatigue test will be used to carry out fatigue – healing – fatigue on asphalt mixture, and then compare the flexural strength and fatigue resistance before and after healing to evaluate the self-healing performance of asphalt mixture with basalt and limestone aggregates. The ultimate purpose of this study is to reveal the mechanism of basalt microwave heating and to prove that asphalt mixture with basalt and limestone aggregates has good microwave self-healing properties.

2. Materials and experimental method

2.1. Bitumen

The bitumen used in this study was 70# base bitumen, and the penetration, ductility and softening point of bitumen were tested according to T0604-2011, T0605-2011 and T0606-2011 in Standard test methods of bitumen and bituminous mixtures for highway engineering (JTG E20-2011) [42]. The performance test results were that the penetration of the bitumen at 25 °C was 70.6 dmm, the ductility of the bitumen at 10 °C was 40.5 cm, and the softening point measured by the ring and ball method was 47.5 °C. Its three major indicators were in line with the relevant requirements in Technical Specifications for Construction of Highway Asphalt Pavements (JTG F40-2004) [43].

2.2. Aggregates

The aggregates used were basalt with the particle size of 5–10 mm and 10–15 mm, and limestone with the particle size of 0–5 mm, 5–10 mm and 10–15 mm. Test method was Test Methods of Aggregate for Highway Engineering (JTG E42-2005) [44]. All technical indexes of the aggregates were used to meet the requirements of JTG E40-2004. The technical parameters are shown in Tables 1–3.

2.3. Filler

The filler used is limestone mineral powder, and all its technical parameters meet the requirements of JTG E20-2004. The test results are shown in Table 4.

2.4. Test method for aggregates characterization

2.4.1. Chemical composition test of aggregates

The chemical composition of basalt powder and limestone powder samples was tested by the ARL PERFORM'X instrument. The test principle was X-ray fluorescence spectrometry (XRF), the test method was the conventional tablet method, and the test mode was oxide.

2.4.2. Elemental analysis test of basalt

The basalt was analyzed and tested by X-ray photoelectron spectrometer (Thermo Fischer, ESCALAB 250Xi, USA). Before the test, the samples were thinned by 1 mm etching spot using an argon ion gun, and the test parameters were set, and then the basalt samples were tested.

2.4.3. Phase composition test of aggregates

The phase composition of basalt powder and limestone powder was tested by the Bruker D8 advance instrument, and the technical principle was X-ray diffraction (XRD). After setting the test parameters of the instrument (the test range is 10°–80°, the scanning speed is 5°/min), the phase composition test can be started.

2.4.4. Electromagnetic performance test of basalt

The electromagnetic parameters of the basalt were tested by a microwave vector network analyzer (MVNA), the instrument model was Agilent E5071C. After setting the test parameters of the instrument (test range 1–18 GHz, coaxial method), the electromagnetic parameter test can be started.

Table 1
Technical parameter of limestone coarse aggregates.

Testing parameters	Testing Results	Technical indicators	Experiment method
Apparent relative density	2.674	≥ 2.5	JTG E42-2005T0605
Water absorption (%)	0.5	≤ 2.0	JTG E42-2005T0308
Crushing value (%)	22.2	≤ 28	JTG E42-2005T0316
Los Angeles abrasion (%)	15.6	≤ 2 8	JTG E42-2005T0317

Table 2
Technical parameter of limestone fine aggregates.

Testing parameters	Testing Results	Technical indicators	Experiment method
Apparent relative density	2.712	≥ 2.5	JTG E42-2005T0328
Angularity (s)	38	≥ 30	JTG E42-2005T0345
Sand equivalent (%)	72.4	≥ 60	JTG E42-2005T0334

Table 3
Technical parameter of basalt coarse aggregates.

Testing parameters	Testing Results	Technical indicators	Experiment method
Apparent relative density	3.070	≥ 2.5	JTG E42-2005T0605
Water absorption (%)	1.08	≤ 2.0	JTG E42-2005T0308
Crushing value (%)	11.4	≤ 28	JTG E42-2005T0316
Los Angeles abrasion (%)	8.1	≤ 28	JTG E42-2005T0317

Table 4
Test results and specifications of limestone powder.

Testing parameters		Testing Results	Technical indicators	Experiment method
Moisture content (%)		0.4	≤ 1	Drying method
Relative density		2.678	≥ 2.5	JTG E42-2005T0352
Hydrophilic coefficient		0.76	< 1	JTG E42-2005T0353
Plastic coefficient		3.4	< 4	JTG E42-2005T0354
Particle size range	< 0.6 mm	100	100	JTG E42-2005T0351
	< 0.15 mm	93.2	90–100	
	< 0.075 mm	84.6	75–100	

2.5. Mix ratio design of asphalt mixture

Fig. 1 shows the design results of the AC-13 limestone asphalt mixture and the design results of the AC-13 asphalt mixture with basalt and limestone aggregates. The manufacturing process of Marshall specimens was performed according to T 0702-2011 in JTG E20-2011. The parameters of the asphalt mixture Marshall test specimens are shown in Table 5. The limestone mass in the limestone asphalt mixture was 94.2% of the total mass. Asphalt mixture with basalt and limestone aggregates used basalt as coarse aggregates and limestone as fine aggregates. The mass of limestone was 45% of the total mass, and the mass of basalt was 54% of the total mass.

2.6. Test methods for asphalt mixture

2.6.1. Heating rate test of aggregates

Limestone with a particle size of 5–10 mm, basalt with a particle size of 5–10 mm and a particle size of 10–15 mm were prepared, and 300 g of aggregates of each particle size were prepared and put into cartons. The emissivity of the thermal imager was 0.95. The heating rate of aggregates was tested after microwave heating for 0–80 s, with each data interval of 10 s. At the end of each heating, the thermal image of the

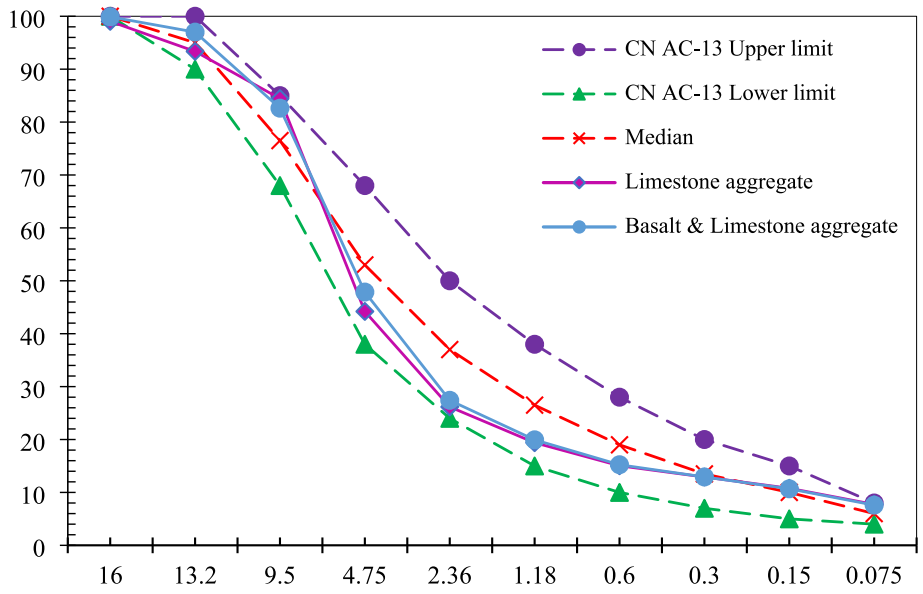

Fig. 1. Asphalt mixture gradation curve.

Table 5
Asphalt mixture design parameters.

Aggregate	10–15 (mm)	5–10 (mm)	0–5 (mm)	Mineral powder	Bituminous binder content
Limestone	17.0%	37.0%	45.0%	1.0%	4.8%
Basalt & Limestone	21.0%	33.0%	45.0%	1.0%	4.8%

surface of the aggregate shall be quickly intercepted, and the average temperature of the surface of the aggregate shall be taken as the temperature value of the heated aggregates.

2.6.2. Heating rate test of asphalt mixture

Under the microwave power of 800 W, microwave heating experiments were carried out on asphalt mixture with basalt and limestone aggregates and limestone asphalt mixture. Two kinds of asphalt mixture Marshall specimens were sliced, the size of cylinder specimens was 25.0 mm in height and 101.5 mm in diameter. The temperature change of the asphalt mixture was tested after microwave heating for 0–120 s, with each data interval of 30 s. At the end of each heating, the temperature distribution map of the asphalt mixture specimen surface shall be intercepted with a thermal imager, and the average temperature of the specimen surface shall be used as the temperature value of the heated specimens. To reduce the error caused by different test specimens, one sample of each asphalt mixture was prepared. To reduce the error caused by the different initial temperatures of the test specimens during each measurement, the surface temperature of the test specimens was recorded before the start of the test, and the difference between the average temperature and the initial temperature of the test specimens was calculated after each temperature measurement, and the surface temperature of the test specimens was superimposed on the basis of 15 °C, to obtain accurate temperature rise data. After each measurement, it needed to stand for 4 h and cool to room temperature, and then test the next group of data.

2.6.3. Self-healing performance test of asphalt mixture

(1) −10 °C SCB test

SCB test was used to carry out fracture–healing–fracture on asphalt mixture. Before the start of the SCB test, special specimens for the SCB test should be prepared, and the Marshall specimens of the asphalt mixture with basalt and limestone aggregates and the limestone asphalt mixture should be processed respectively. The specimens for the SCB test shall be a semi-cylinder with a height of 63.5 mm, and the sides are standard semicircles with a radius of 50.8 mm. In order for the asphalt mixture to be evenly split in half and have a fracture surface suitable for healing, a slit with a size of 2.0 mm × 2.0 mm × 63.5 mm was cut on the cut surface of the asphalt mixture. Four specimens were selected from each asphalt mixture specimen, eight in total, and their microwave heating self-healing properties were tested after fracture at −10 °C. Before the test, 3 specimens were taken from each of the 2 asphalt mixture specimens and held at −10 °C for more than 4 h. After 4 h, the specimens were subjected to the SCB test using a universal testing machine (UTM). The loading rate of the UTM test was 0.5 mm/s, the test temperature was −10 °C, and the instrument automatically recorded the fracture data. The fractured specimens were squeezed hard and allowed to stand at room temperature for 2 h. The specimens were then wrapped tightly with heat-resistant tape, and they were left to stand at room temperature for 4 h. After standing for 4 h, the specimens were placed in a microwave oven for heating for 120 s. After heating, the specimens were taken out and left at room temperature for 12 h. After cooling to room temperature, continued to hold at the −10 °C for more than 4 h. After 4 h, continued to use UTM to perform SCB testing on the samples with the same test parameters as before. So far, one microwave healing cycle of the asphalt mixture has been completed. According to the above healing test process, 7 fracture tests and 6 microwave heating processes of 120 s (6 microwave healing cycles) were carried out on the two asphalt mixtures. The specific test process is shown in Fig. 2.

After the SCB test using UTM, the maximum fracture force and fracture energy data of the asphalt mixture specimens can be obtained respectively. The microwave healing rate of the asphalt mixture can be calculated from the maximum fracture force and fracture energy of the asphalt mixture specimens, respectively, and the equations of the healing rate are shown in Eqs. (3) and (4).

$$H_{fi} = \frac{F_i}{F_0} \times 100\% \tag{3}$$

$$H_{ei} = \frac{E_i}{E_0} \times 100\% \tag{4}$$

H_{fi} is the healing ratio after the i-th failure calculated by the maximum fracture force,H_{ei} is the healing ratio after the i-th failure calculated by

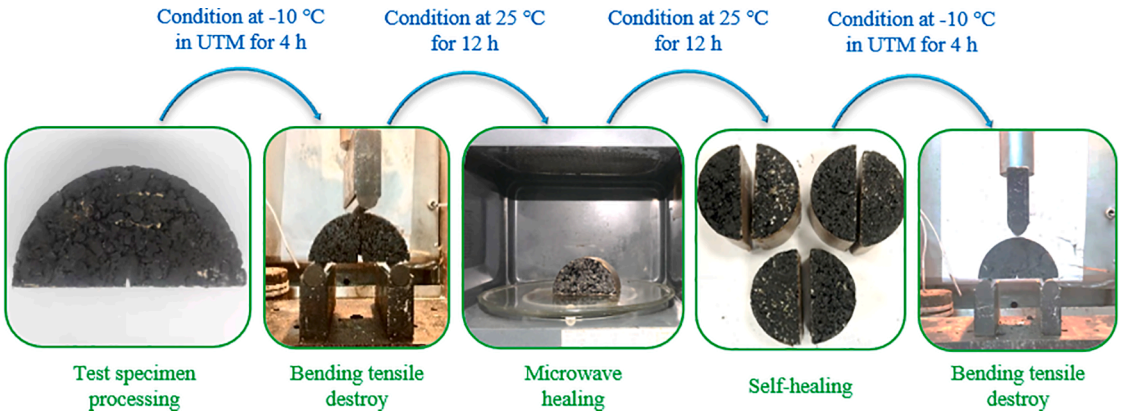

Fig. 2. SCB test and microwave healing of asphalt mixture.

the fracture energy, F_0 and E_0 are the initial (first failure) maximum fracture force and fracture energy of the asphalt mixture specimens respectively, F_i and E_i are the maximum fracture force and fracture energy of the asphalt mixture after the i-th healing of the asphalt mixture specimens respectively. During subsequent data analysis,H_{fa} is the average healing ratio calculated by the maximum fracture force, H_{ea} is the average healing ratio calculated from fracture energy.

(2) 25 °C fatigue test

The fatigue test was used to carry out fatigue–healing–fatigue on asphalt mixture. Before the fatigue test starts, special specimens for the fatigue test should be prepared, which were the same as those used in the SCB test. Four samples were selected from each of the two mixture samples, and their microwave heating self-healing properties were tested after the fatigue test at 25 °C. Before the test, 5 specimens were taken from each of the two asphalt mixtures and held at 25 °C for more than 4 h. After 4 h of heat preservation, one specimen was taken from each of the two asphalt mixtures, the SCB test was performed on them using UTM, and the two maximum axial force data were recorded. Based on the 2 maximum axial forces that have been obtained, with a stress ratio of 0.5, the other 4 specimens of each group were subjected to 25 °C fatigue tests using UTM, and their failure times were recorded separately. The healing process was the same as in the SCB test, except that the test temperature was different. The above test process was repeated, and a total of 5 times of fatigue tests, 4 times of microwave heating healing, and 4 microwave healing cycles were performed on the 2 kinds of asphalt mixtures.

After using UTM for the fatigue test, the failure times of the asphalt mixture can be obtained. The microwave healing rate of the asphalt mixture is calculated by the number of failure times of asphalt mixture specimens. The calculation of the healing rate is shown in Eq. (5).

$$H_{ni} = \frac{N_i}{N_0} \times 100\% \tag{5}$$

H_{ni} is the healing ratio after the i-th calculated by the number of failures, N_0 is the initial (the first fatigue) failure times of asphalt mixture specimens, N_i is the failure times of the asphalt mixture after the i-th healing of the asphalt mixture specimens. During subsequent data analysis, H_{na} is the average healing ratio calculated by the number of failures.

2.7. Technical map

Fig. 3 is the technical map of this study.

3. Results and discussions

3.1. Microwave heating mechanism of aggregates

3.1.1. Chemical composition of aggregates

Table 6 shows the test results of element content in basalt. There were 27 elements detected, and the table lists 8 elements with a content of more than 1%, namely Si, Fe, Ca, Al, Mg, Ti, Na and K. These elements constitute an important part of basalt. There were 19 elements in basalt whose content was less than 1%, namely P, Mn, Sr, S, V, Ba, Cl, Zr, Cu,

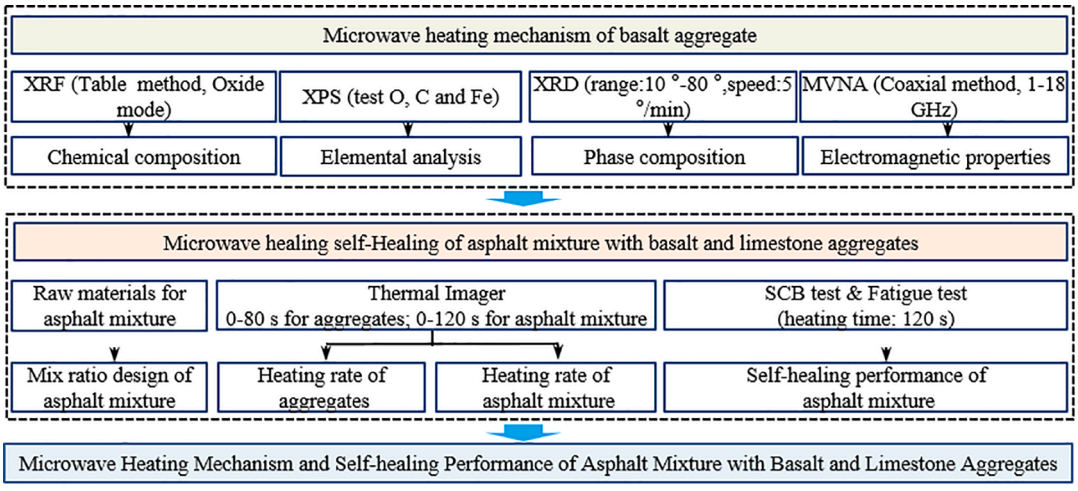

Fig. 3. Technical map.

Table 6
Element content of basalt.

Element	Si	Fe	Ca	Al	Mg	Ti	Na	K	Other
Wt (%)	17.92	12.92	10.89	5.39	5.77	1.14	1.37	1.48	44.22

Zn, Co, Cr, Ni, Nd, Ag, Gd, Y, Rb and Ga. In the first 8 elements, there were 7 kinds of metallic elements, while the non-metallic elements had only one Si element. Among the first three elements, Si had the largest content, accounting for 17.92% by mass, which was close to the sum of Fe and Mg. The second element was Fe, with a mass ratio of 12.92%, which was close to the sum of the contents of Ca and K elements. The last element was Ca, accounting for 10.89% by mass, which was close to the sum of the contents of Al and Mg elements. The five most abundant elements accounted for more than half of the total mass of basalt.

Table 7 shows the test results of element content in limestone. There were 21 elements detected, and the table lists 2 elements with a content of more than 1%, namely Ca and Mg, which constitute an important part of limestone. There were 19 elements in limestone whose content was less than 1%, namely Fe, Si, Mn, P, F, Al, Na, Sn, S, Sr, K, Ti, Cl, Cr, Ag, Zn, Ni, Cu, and Pb, it was worth noting that Fe content is only 0.54%. The two elements with content of more than 1% were all metallic elements, the total content of Ca and Mg reached 66.26% by mass.

Table 8 shows the test results of oxide content in basalt. There were 27 kinds of oxides detected, and 9 kinds of oxides with a content of more than 1% were listed in the table. They were SiO_2, Fe_2O_3, CaO, Al_2O_3, MgO, TiO_2, Na_2O, K_2O and P_2O_5, seven of which were metallic oxides, which were important components of basalt. There were 18 elements with oxide content below 1% in basalt, namely MnO, SrO, SO_3, V_2O_5, BaO, Cl, ZrO_2, CuO, ZnO, Co_3O_4, Cr_2O_3, NiO, Nd_2O_3, Ag_2O, Gd_2O_3, Y_2O_3, Rb_2O and Ga_2O_3. Among the top three oxides, the content of SiO_2 was relatively high, with a mass ratio of 38.40%, which was twice that of Fe_2O_3, and was close to the sum of Fe_2O_3, CaO, TiO_2, Na_2O and K_2O. The mass ratio of Al_2O_3 and MgO was similar, both were about 10%. The masses of TiO_2, Na_2O, K_2O and P_2O_5 were also close to each other, and the mass ratio was about 2%.

Table 9 shows the test results of oxide content in limestone. There were 21 kinds of oxides detected, and 2 kinds of oxides with a content of more than 1% were listed in the table. They were CaO and MgO, both metallic oxides, which are important components of limestone. There were 19 elements with oxide content below 1% in limestone, namely Fe_2O_3, SiO_2, MnO, P_2O_5, F, Al_2O_3, Na_2O, SnO_2, SO_3, SrO, K_2O, TiO_2, Cl, Cr_2O_3, Ag_2O, ZnO, NiO, CuO, and PbO, it was worth noting that Fe_2O_3 content was only 0.77%. The two oxides with content of more than 1% were all metallic oxides, the total content of CaO and MgO reached 97.11% by mass.

The comprehensive analysis of the chemical composition of basalt and limestone shows that 97.11% of the limestone mass was CaO and MgO, while the microwave absorbing performance of limestone is poor, which indicates that Ca and Mg elements have only a small promotion effect on microwave heating of the material. The chemical composition analysis of basalt shows that the five elements (or oxides) with the highest content were Si, Fe, Ca, Al and Mg (or their oxides). Due to basalt has excellent wave-absorbing properties, the influence of Ca and Mg elements was excluded, which shows that the excellent wave-absorbing properties of basalt are highly correlated with elements such as Si, Fe and Al.

Table 7
Element content of limestone.

Element	Ca	Mg	Other
Wt (%)	49.15	17.11	33.74

3.1.2. Element analysis of basalt

The content of the Fe element was the highest among the metal elements contained in basalt, and the content of Fe_3O_4 was second only to SiO_2 in all oxides contained in basalt, accounting for 18.5%. Fe_3O_4 is not a pure oxide, and its chemical formula is Fe_2O_3·FeO, that is, the valence states of Fe elements in Fe_3O_4 are divalent and trivalent. Fe_3O_4 has strong microwave-absorbing properties. Fe_3O_4 is a strong magnetic material and Fe_2O_3 is a weak magnetic material [45,46]. It can be seen that Fe_3O_4 with Fe^{2+} has strong magnetism and Fe^{2+} is more sensitive to microwave than Fe^{3+}. The effect of the valence state of the Fe element on the microwave heating of basalt was analyzed by X-ray photoelectron spectroscopy (XPS).

Figs. 4 and 5 show the results of C1s and O1s peaks in the XPS spectrum of basalt. The C element on the surface of basalt powder can exist in four forms: C=O, C–O, C=C and C–C, and its (peak center position) binding energies were 284.80 eV, 286.29 eV, 287.73 eV and 289.11 eV respectively. The O element on the surface of basalt powder existed in three forms: lattice oxygen (O_L), adsorbed oxygen (O_H) and oxygen vacancy (O_V), and its (peak center position) binding energies were 529.97 eV, 531.27 eV and 532.67 eV respectively. Table 10 and Table 11 list the peaks, peak areas and relative content data of four forms C and three forms O. The C–C form had the highest peak area and relative content of C element, the peak area was 11685.89, and the relative content proportion is 63.05%, more than the sum of the other three C forms. The peak area and relative content of O element in the form of adsorbed oxygen were the highest, with a peak area of 157392.6 and a relative content ratio of 77.98%, exceeding the sum of the other three O forms.

Fig. 6 is the Fe2p peak spectrum results in the basalt XPS spectrum. It can be seen from the figure that the C element on the surface of basalt powder can exist in four forms: Fe^{2+} $2p_{3/2}$, Fe^{2+} $2p_{1/2}$, Fe^{3+} $2p_{3/2}$ and Fe^{3+} $2p_{1/2}$. Fe^{2+} $2p_{3/2}$ is the energy level of divalent iron $2p_{3/2}$, and its (peak center position) binding energies were 708.66 eV, 721.76 eV, 710.32 eV and 723.70 eV respectively. There were satellite peaks (characteristic peaks) in the four forms of Fe^{2+} $2p_{3/2}$, Fe^{2+} $2p_{1/2}$, Fe^{3+} $2p_{3/2}$ and Fe^{3+} $2p_{1/2}$, which were used to help determine the valence state of some metals. The four satellite peaks of Fe^{2+} $2p_{3/2}$, Fe^{2+} $2p_{1/2}$, Fe^{3+} $2p_{3/2}$ and Fe^{3+} $2p_{1/2}$ of Fe element have binding energies of 712.89 eV, 727.42 eV, 716.42 eV and 732.44 eV respectively. Table 12 lists the peak value, peak area and relative content data of the two Fe valence states. In basalt, the relative content of Fe^{3+} was 68.95%, the relative content of Fe^{2+} was 31.05%, the content of Fe^{3+} was greater than that of Fe^{2+}, and the content of Fe^{3+} was 2.22 times that of Fe^{2+}. Because Fe^{2+} can react with oxygen in the air to form Fe^{3+} [46], so the content of Fe^{3+} will be higher than that of Fe^{2+}. With the increase of time, the Fe^{2+} content in the basalt keeps decreasing, while the Fe^{3+} content keeps increasing, which makes the magnetic properties of the basalt worse and worse, which is not conducive to absorbing waves and generating heat.

3.1.3. Phase composition of aggregates

Fig. 7 shows the XRD qualitative analysis results of basalt. Four phases were detected in the basalt powder samples, the main phase was Actinolite (JCPDS 89-5366), and the secondary phases were Albite high (JCPDS 75-1142), Epidote (JCPDS 75-1142) and Chlorite-serpentine (JCPDS 52-1044), represented by ♠, ♥, ♣ and◆ patterns respectively.

Fig. 8 shows the XRD qualitative analysis results of limestone. Three phases were detected in the limestone powder samples, the main phase was Dolomite (JCPDS 75-1760), and the secondary phases were Albite (JCPDS 09-0466) and Calcite (JCPDS 83-0577), represented by ♠, ♥ and

Table 8
Oxide content of basalt.

Oxide	SiO_2	Fe_2O_3	CaO	Al_2O_3	MgO	TiO_2	Na_2O	K_2O	P_2O_5	Other
Wt (%)	38.34	18.48	15.24	10.19	9.58	1.90	1.84	1.79	1.77	0.87

Table 9
Oxide content of limestone.

Oxide	CaO	MgO	Other
Wt (%)	68.74	28.37	2.89

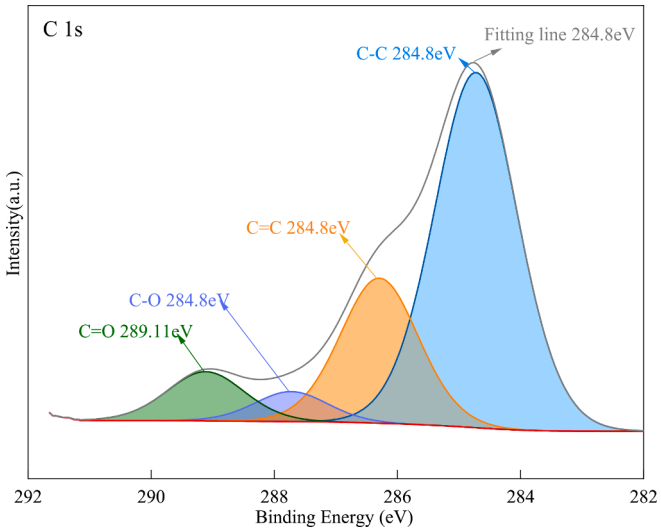

Fig. 4. C1s peak spectrum in basalt XPS spectrum.

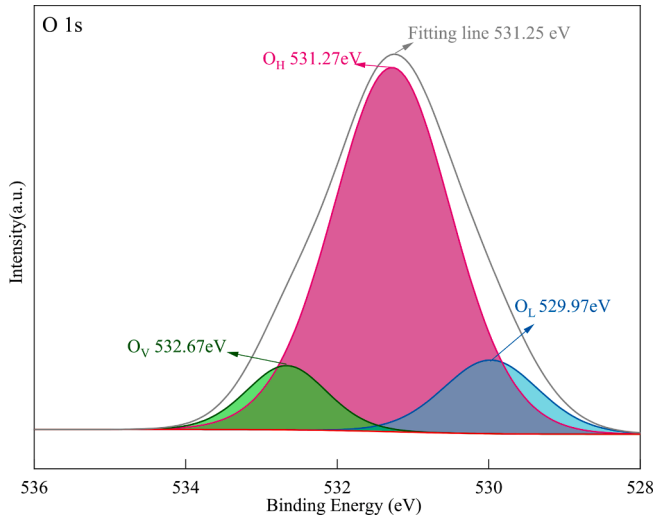

Fig. 5. O1s peak spectrum in basalt XPS spectrum.

Table 10
Contents of different valence states of C element.

Name	Peak BE (eV)	FWHM (eV)	Area (P) CPS.	Atomic (%)
C–C	284.80	1.60	11685.89	63.05
C=C	286.29	1.50	4478.26	24.17
C–O	287.73	1.40	868.58	4.69
C=O	289.11	1.48	1496.77	8.09

Table 11
Content of O element in different valence states.

Name	Peak BE (eV)	FWHM (eV)	Area (P) CPS.	Atomic (%)
O_L	529.97	1.49	25653.42	12.70
O_H	531.27	1.85	157392.60	77.98
O_V	532.67	1.25	18791.09	9.32

♣ patterns respectively.

Si has dielectric properties and absorbs microwaves by means of dielectric loss [29,47,48]. Ferrite has both dielectric loss and magnetic loss, and absorbs microwave energy mainly through magnetic loss [49,50]. Some studies have pointed out that the compounds composed of Si and related metals such as Fe and Al have good electromagnetic properties and can absorb microwaves [51,52]. Among the three phases of limestone, the second phase was related to Si and Al compounds. Among the four phases of basalt, they can be split into ferrite and Si combinations, or Si, Fe and Al combinations. Because of the presence of these two substances, basalt can be heated by microwaves, and its microwave heating performance was better than that of limestone.

3.1.4. *Electromagnetic properties of basalt*

Fig. 9 shows the test results of dielectric loss tangent and magnetic loss tangent. In the microwave frequency range of 1–18 GHz, the dielectric loss tangent and magnetic loss tangent of basalt all decrease with the increase of frequency, and the loss ability to microwaves decreases continuously. In the microwave frequency range of 1–18 GHz, the magnetic loss tangent was always slightly larger than the dielectric loss tangent. The main way for basalt to absorb microwaves to generate heat was the magnetic loss, but the dielectric loss also contributes to a certain extent. Fig. 10 shows the loss tangent test results of basalt. It can be seen that the loss of basalt to microwave generally decreases with the increase of microwave frequency in the range of 1–18 GHz.

Fig. 11 shows the test results of the real and imaginary parts of the basalt dielectric constant. The value of ε' and ε" of the basalt dielectric constant showed a fluctuating decrease as a whole, which indicated that the basalt had charge transport and dielectric loss under the action of microwaves. Under the action of microwave, the electric storage capacity and electric loss capacity of basalt weaken with the increase of frequency. The value ε' of basalt decreases substantially in the microwave frequency range of 1–1.13 GHz, and fluctuates in the microwave frequency range of 1.13–18 GHz. The value of ε' of the dielectric constant fluctuates around 3 as a whole. The value of ε" showed a fluctuating decrease as a whole, it rose sharply in the range of 1–1.13 GHz, and fluctuates in the range of 1.13–18 GHz. Fig. 12 shows the test results of the real and imaginary parts of the basalt permeability. The value μ" of basalt decreased with the increase of frequency as a whole, indicating that under the action of microwave, the magnetic storage capacity and magnetization capacity of basalt weaken with the increase of frequency.

Si is an electrical loss absorbing material, and many ferrites are magnetic loss absorbing materials. It can be seen that the reason why basalt is a magnetic loss absorbing material is inseparable from a high proportion of metal elements. The combination of magnetic loss materials and electrical loss materials makes the whole material have both dielectric loss and magnetic loss capabilities, which is beneficial to improving its microwave-absorbing properties [53]. The composite of ferrite and Si in basalt results in strong microwave-absorbing properties. Therefore, the use of basalt coarse aggregates instead of limestone coarse aggregates can enhance the overall dielectric loss performance

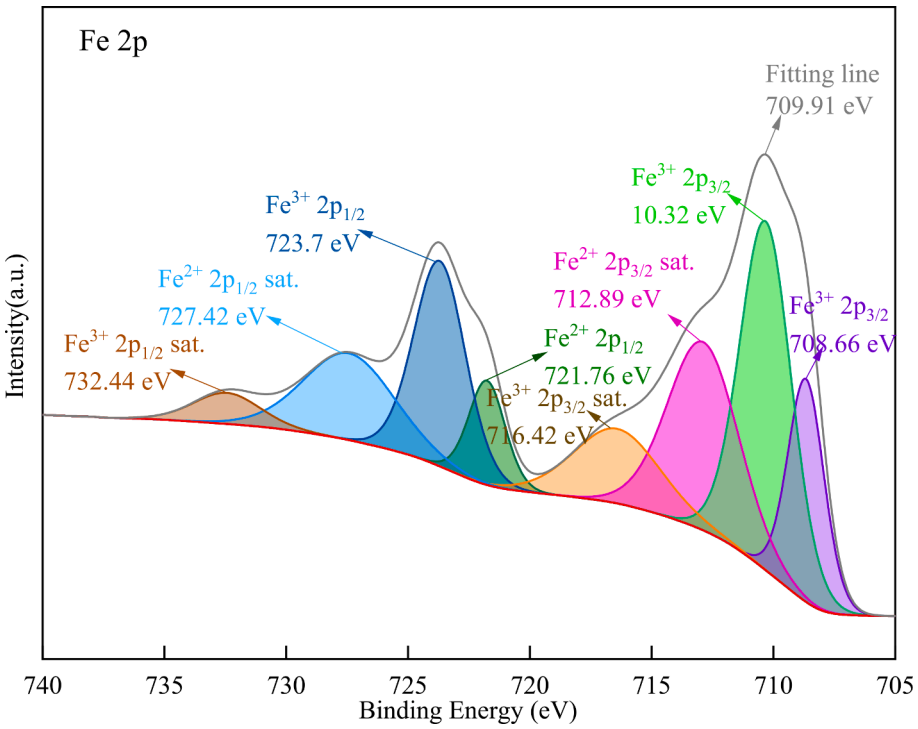

Fig. 6. Fe2p peak spectrum in basalt XPS spectrum.

Table 12
The content of Fe elements in different valence states.

Name	Peak BE (eV)	FWHM (eV)	Area (P) CPS.	Atomic (%)
Fe^{2+} $2p_{3/2}$	708.66	1.76	5087.31	31.05
Fe^{2+} $2p_{1/2}$	721.76	1.76	2380.15	
Fe^{3+} $2p_{3/2}$	710.32	2.49	11285.04	68.95
Fe^{3+} $2p_{1/2}$	723.70	2.49	6641.72	

and magnetic loss performance of the asphalt mixture. Under the action of microwave, asphalt mixture will quickly absorb the microwave and generate heat. The microwave absorbing mechanism of basalt provides a theoretical basis for the follow-up study of the feasibility of self-healing of asphalt mixtures under the action of microwaves.

3.1.5. *Electromagnetic loss performance of basalt*

The RL determines the final absorbing performance of the absorbing material, and the RL is negatively correlated with the absorbing performance of the material [32]. The maximum absorption and attenuation of electromagnetic waves by the microwave absorbing material at the current microwave frequency and material thickness can be studied according to the magnitude of the RL value (the RL value is all less than 0). When the RL value of the microwave absorbing material is greater than −5 dB, it can only absorb and attenuate up to 68% of the electromagnetic wave. When the RL value of the absorbing material is less than −10 dB, the microwave absorbing material can absorb and attenuate more than 90% of the electromagnetic waves. The microwave frequency range in which the absorbing material can absorb and attenuate more than 90% of electromagnetic waves is called the effective bandwidth [34,37].

Fig. 13 shows the effect of basalt powder thickness on microwave reflection loss. The RL values of basalt powder with different thicknesses fluctuated in the microwave frequency range of 1–18 GHz, indicating that the absorbing properties of basalt changed with the microwave frequency and material thickness. When the thickness of the basalt powder coating was 4.0 mm, the maximum absorption and attenuation of electromagnetic waves occurs, and the RL value was about −2.2 dB. Currently, only in the microwave frequency range of 1–18 GHz, the difference between the permittivity and permeability of basalt was small, and the frequency had little effect on the absorbing performance of basalt. Among them, when the thickness of the basalt powder coating was less than or equal to 1.0 mm, the numerical fluctuation was less obvious. When the thickness of the basalt powder coating was less than or equal to 4.0 mm, the frequency range where the RL was lower than −5 dB does not appear on the RL curve. This showed that when the thickness of the basalt powder coating was less than or equal to 4.0 mm, only 68% of the microwave can be absorbed and attenuated, and the absorption and attenuation of 90% cannot be achieved, and there was no effective bandwidth. The thicker the basalt coating, the smaller the reflection loss point and the better the microwave absorbing performance. Theoretically, when the density is the same, the basalt with large particle size absorbs the microwave better than the basalt with smaller particle size. It can be seen that when the thickness of basalt powder coating was less than or equal to 4.0 mm, the absorbing performance of basalt was poor, but with the increase of powder thickness, the absorbing performance became better.

3.2. *Microwave heating performance of asphalt mixture*

3.2.1. *Heating rate of aggregates*

Fig. 14 shows the thermal image of the aggregates heating and the test results of its average surface temperature. In the thermal imaging software, after specifying a circular rule for the thermal imaging image, the relevant parameters such as the highest temperature, the lowest temperature and the average temperature in the circular area were obtained.

Fig. 15 shows the test results of the heating rate of basalt and limestone with different particle sizes under the action of microwaves. Under microwave heating conditions, the heating rate of limestone with the particle size of 0–5 mm was 0.4018 °C/s, the heating rate of basalt with the particle size of 0–5 mm was 0.7695 °C/s, and the heating rate of basalt with the particle size of 10–15 was 0.4018 °C/s. 0.7358 °C/s. The

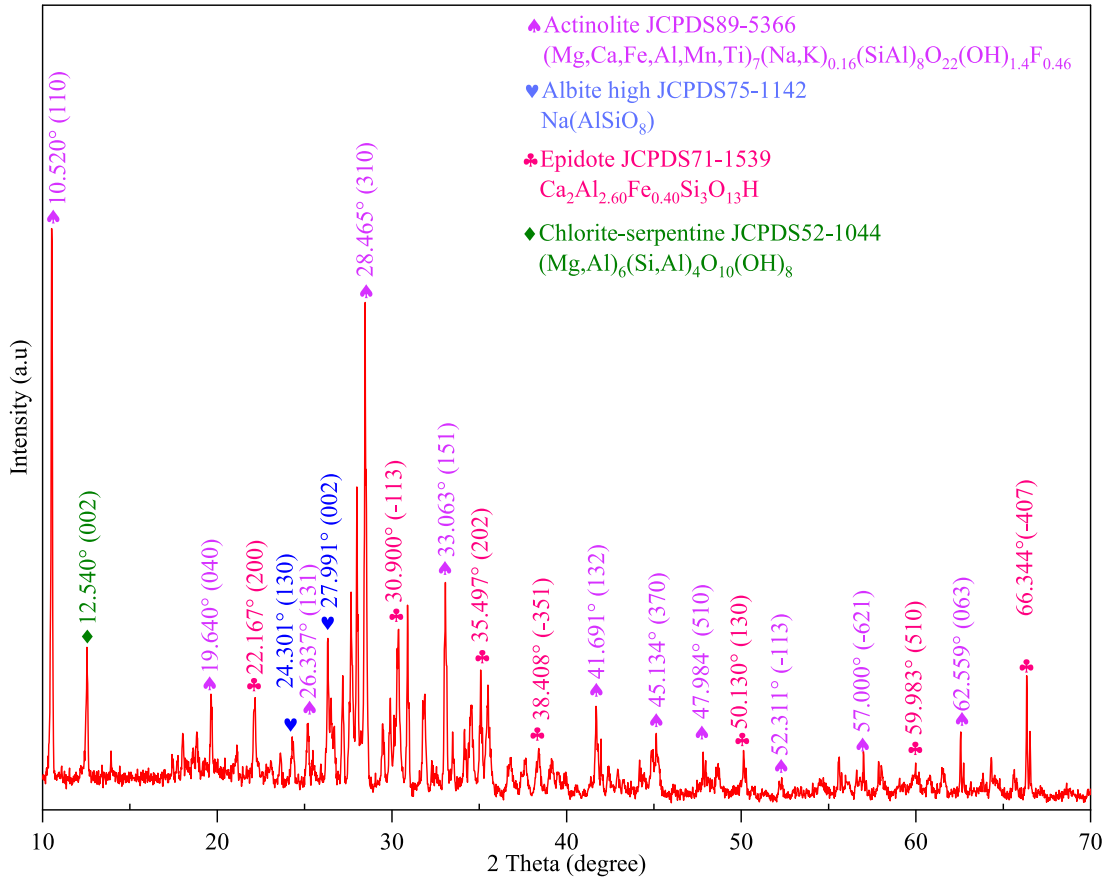

Fig. 7. Qualitative analysis of basalt under XRD.

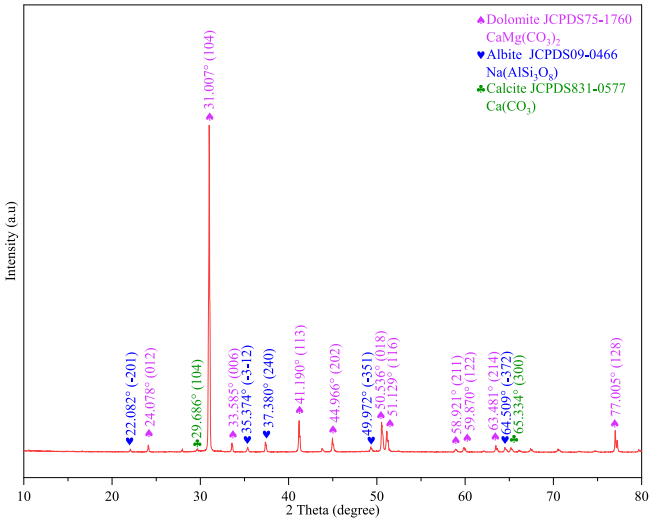

Fig. 8. Qualitative analysis of limestone under XRD.

heating rate of basalt with a particle size of 0–5 mm was 1.91 times that of limestone. The heating rate of basalt with the particle size of 0–5 mm was 1.05 times that of basalt with the particle size of 10–15 mm. It can be seen that under the action of microwaves, the heating rates of basalts with different particle sizes were also slightly different. Due to the better compactness of small-sized basalt in the container, the overall heating rate of small-sized basalt was higher than that of large-sized basalt.

3.2.2. *Heating rate of asphalt mixture*

Basalt heats up quickly under the action of microwave, and through heat transfer, the asphalt around the aggregates can also heat up quickly. The microwave heating of the asphalt mixture with basalt and limestone aggregates and limestone asphalt mixture was carried out to study the effect of basalt on the microwave heating effect of the asphalt mixture. The name of the asphalt mixture with basalt and limestone aggregates is abbreviated as 7BL, and the name of the limestone asphalt mixture is abbreviated as 7L. After microwave heating for different times, the thermal imaging images of the aggregate surface are shown in Fig. 16 and Fig. 17.

Fig. 18 shows the thermal image of the asphalt mixture heating up and the test results of the average temperature of the asphalt mixture surface. The average surface temperature of the two asphalt mixtures heated at 800 W microwave power should be adjusted according to the weight of the mixture and the surface temperature measured each time. Taking the 7BL specimens as the mass benchmark, the actual temperature rise value of the 425 g asphalt mixture after each temperature measurement was calculated, and the initial temperature was calculated at 15 °C. And in Fig. 18, it can be seen that there was a local overheating area in the asphalt mixture. The aggregates in the mixture have different particle sizes and uneven distribution, and the distribution of Fe^{3+} in basalt is also uneven. Due to the good response of Fe to microwaves, the asphalt mixture was prone to overheating under microwave heating conditions. In general, the overheating phenomenon occurred in a small area, and did not have a great impact on the self-healing of the asphalt mixture.

Fig. 19 shows the difference in the surface morphology of the specimens under multiple microwave irradiation. After repeated irradiation for 6 times under the microwave condition with a duration of 2 min and a frequency of 800 W, the basalt heats up rapidly, and the high

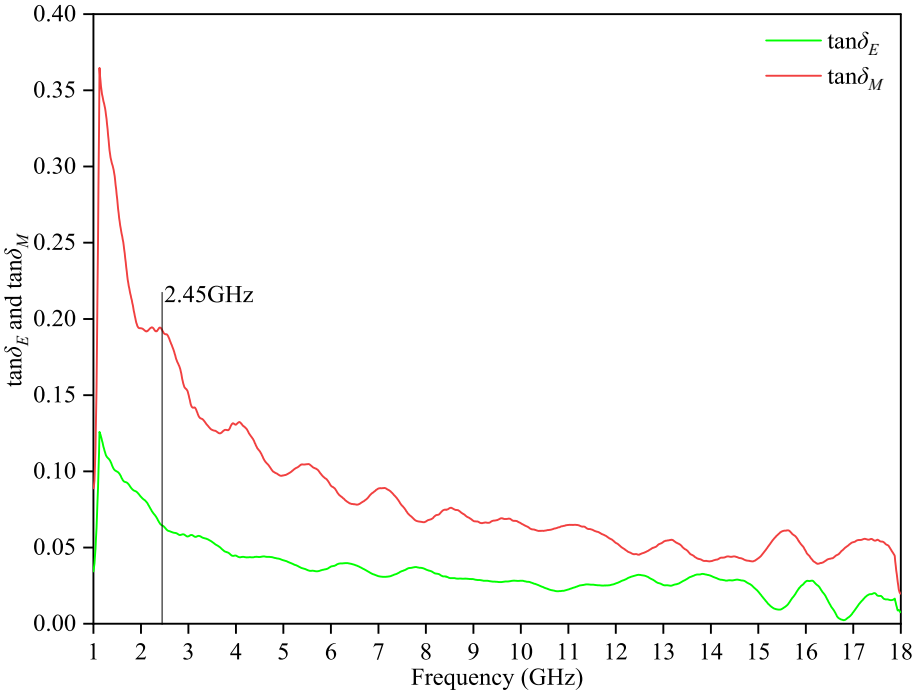

Fig. 9. Basalt dielectric loss tangent and magnetic loss tangent test results.

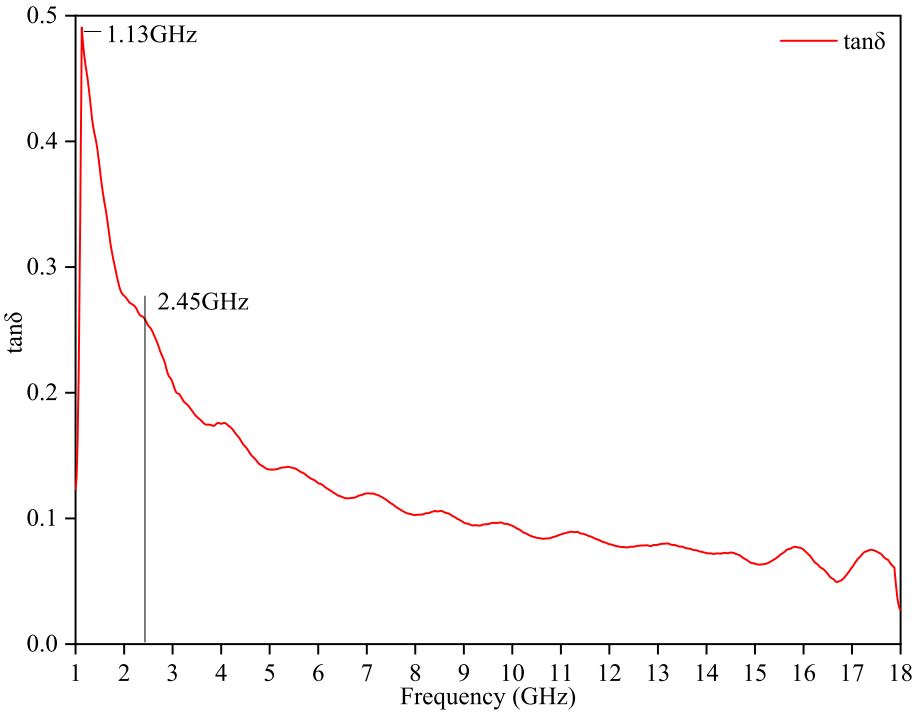

Fig. 10. Basalt loss tangent test results.

temperature causes a large amount of asphalt to gush out of the aggregates gap. However, the temperature of limestone rose slowly, and only less asphalt was gushed out of the aggregate gap compared with the previous specimens. Therefore, the black block on the surface of the sample of asphalt mixture with basalt and limestone aggregates was larger and darker than that of the limestone asphalt mixture. Under the action of microwave, basalt played a great role in promoting the rapid heating of the specimens.

Fig. 20 shows the effect of basalt on the heating rate of the asphalt mixture under microwave heating. From the heating trend, the heating rate curve showed a nonlinear change, indicating that the heating process of the asphalt mixture under the action of microwave is a nonlinear change and the temperature distribution is uneven [54]. The heating rate of the 7BL specimen under microwave heating was greater than that of the 7L specimen, and the average surface temperature of the 7BL specimen at 120 s was 30.6 °C higher than that of the 7L specimen, indicating that basalt can effectively improve the microwave heating rate of asphalt mixture. According to the fitted linear equation, the

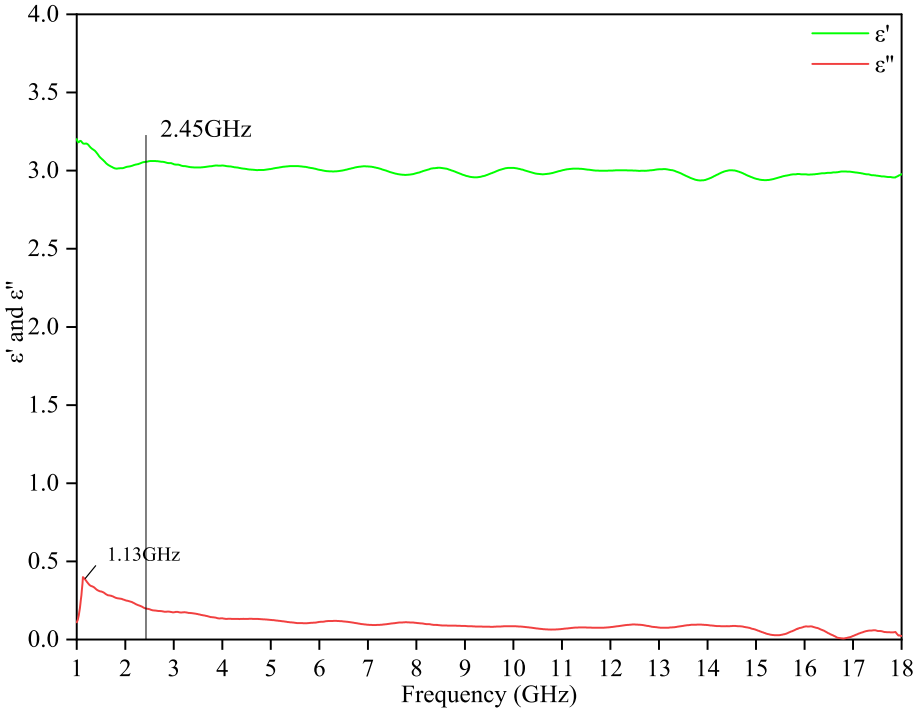

Fig. 11. Test results of real and imaginary parts of basalt dielectric constant.

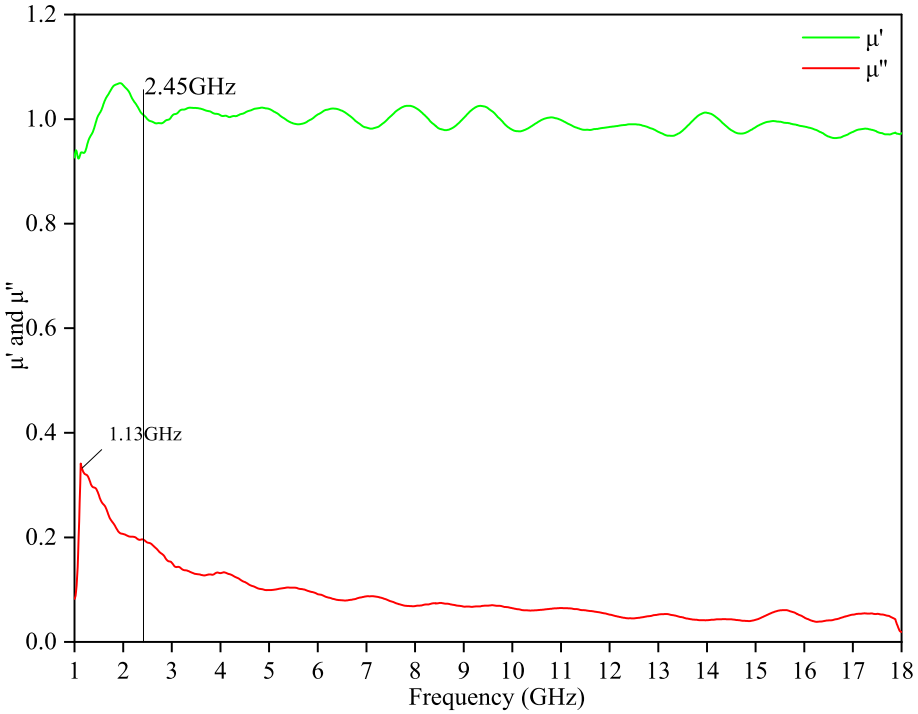

Fig. 12. Test results of real and imaginary parts of basalt permeability.

heating rate of the 7L specimen was 0.54 °C/s, the heating rate of the 7BL specimen was 0.78 °C/s, the heating rate of asphalt mixture with basalt and limestone aggregates was 0.24 °C/s higher than that of limestone asphalt mixture, and the wave-absorbing performance of basalt was better than that of limestone. The heating rate of the 7BL specimen under the action of the microwave was 1.44 times that of the 7L specimen.

3.3. Self-healing properties of asphalt mixture

3.3.1. −10 °C SCB test results

Fig. 21 is a thermal image of the specimen damaged by the SCB test after microwave heating. It can be clearly seen from the figure that the temperature at the crack was higher after microwave heating. On the one hand, because some microwaves were not transmitted or reflected in time after generating heat energy at the cracks of the asphalt mixture,

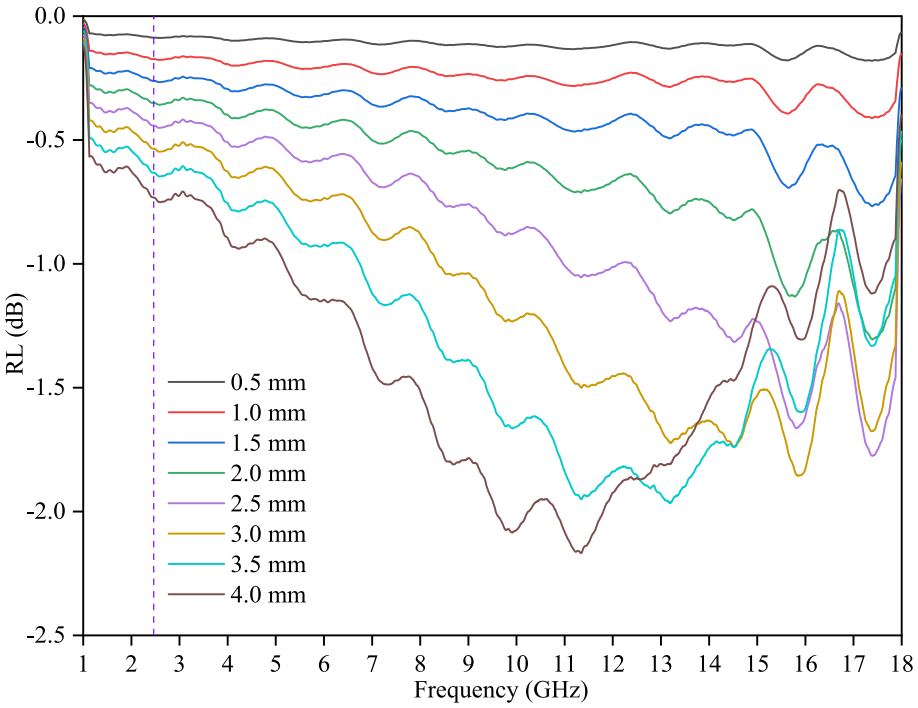

Fig. 13. Effect of basalt powder thickness on microwave reflection loss.

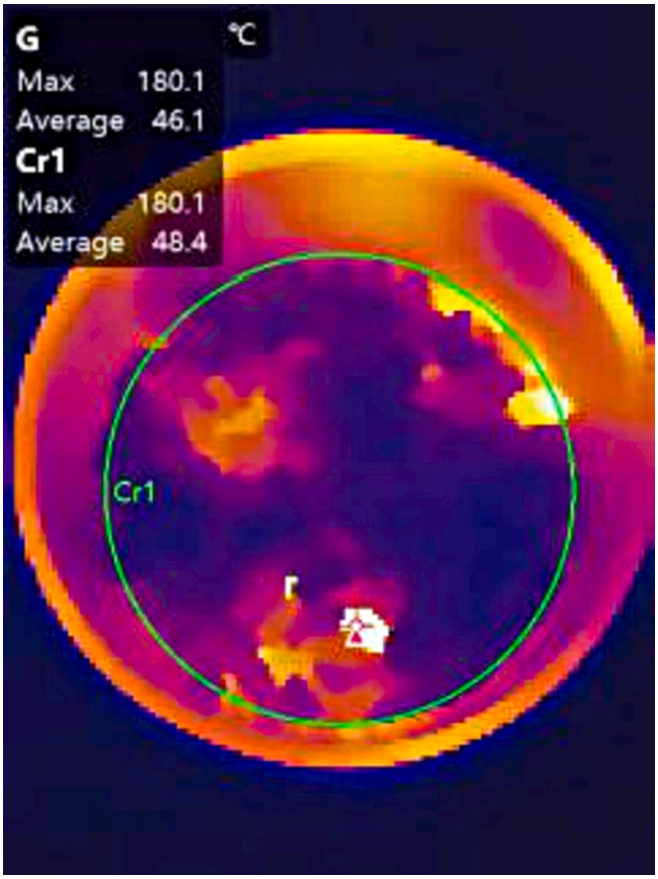

Fig. 14. The thermal image of the aggregates heating and the test results of its average surface temperature.

the absorbing materials in the asphalt mixture continued to absorb the microwaves to generate heat. On the other hand, because the area at the crack was not in direct contact with the outside, when microwave heating, the heat exchange frequency at the crack was low, and the heat was not easily lost, and the heat energy at the crack was efficiently used to heat up the mixture.

Figs. 22 and 23 show the relationship between the number of healing cycles, the H_{ei}, and the H_{fi} in the flexural tensile strength test at −10 °C. The increasing trend of H_{fi} and H_{ei} was roughly the same, and they do not increase or decrease with the increase of healing times. Therefore, it is verified that the longer the microwave heating time and the greater the microwave intensity, only promotes the self-healing of the asphalt mixture, but is not decisive for its self-healing effect. The self-healing properties of asphalt mixtures are only determined by the mixture temperature and temperature duration after microwave heating [55]. Under the action of 800 W microwave for 120 s, the healing effect of each asphalt mixture and the same asphalt mixture after each healing was inconsistent, resulting in different crack temperatures of the heated asphalt mixture. It can be seen from Figs. 22 and 23 that the standard deviation of the fourth healing time was too large, because the size of the asphalt mixture sample may change due to multiple healing times, and the size of a slit in the asphalt mixture may change. With repeated microwave heating, the temperature of the asphalt mixture was high, and the asphalt gushed out from the gap of the aggregates may strengthen the adhesion between bitumen and aggregates, which made the healing rate of a certain specimen for the fourth time was higher than 100%, which in turn led to an excessively large standard deviation of the healing rate. Notably, the microwave healing rate improved overall for the fourth to sixth sessions. This was due to the aging and stiffening of bitumen caused by multiple high temperatures, and then the stiffening of the asphalt mixture. It also experienced multiple structural damages accumulated by volume expansion and contraction. Therefore, the asphalt mixture was prone to SCB test, and its microwave healing rate improved overall.

Fig. 22 shows that the H_{ea} of 7BL is 75.3%, and the H_{ea} of 7L is 25.4%. The H_{ea} of the asphalt mixture containing basalt was significantly higher than that of the asphalt mixture containing only limestone. From the

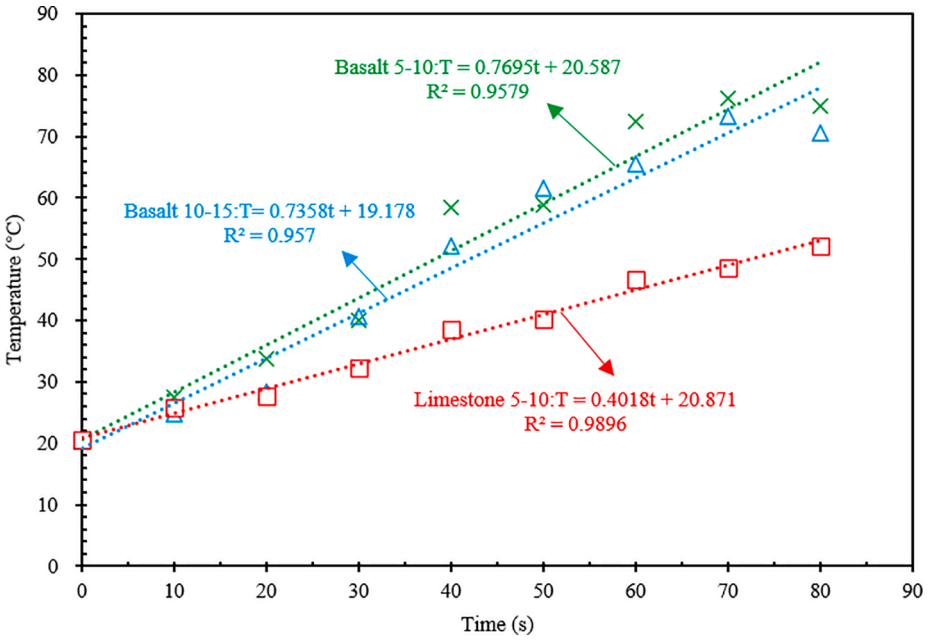

Fig. 15. Microwave sensitivity of basalt and limestone.

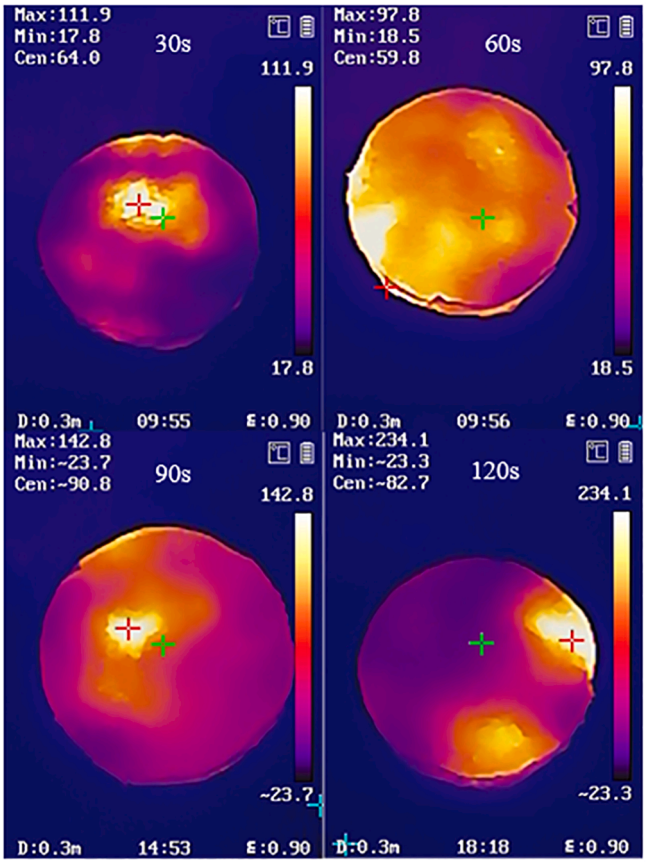

Fig. 16. Thermal image of 7BL.

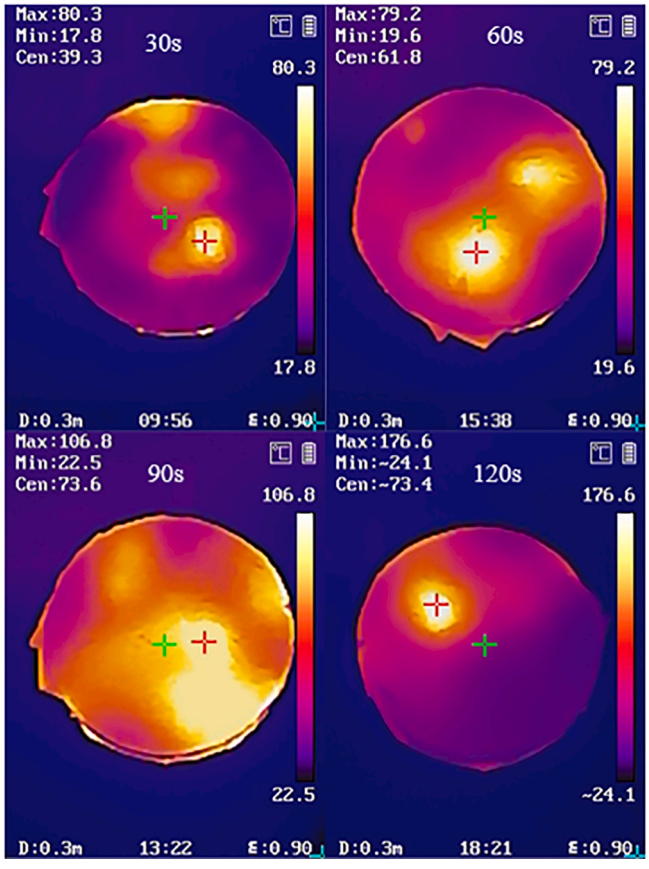

Fig. 17. Thermal image of 7L.

H_{ea}, the self-healing effect of 7BL under the action of the microwave was 2.96 times that of 7L. Fig. 23 shows that the H_{fa} of 7BL is 79.1%, and the H_{fa} of 7L is 36.3%. The H_{fa} of asphalt mixture containing basalt was significantly higher than that of asphalt mixture containing only limestone. From the H_{fa}, the self-healing effect of 7BL under the action of the microwave was 2.18 times that of 7L. After repeated microwave heating and healing, the H_{ei} of 7BL was always maintained above 65%, and the H_{fi} was maintained above 75%. It can be seen that the flexural strength of the asphalt mixture with basalt and limestone aggregates pavement can be recovered by at least 65% by microwave heating.

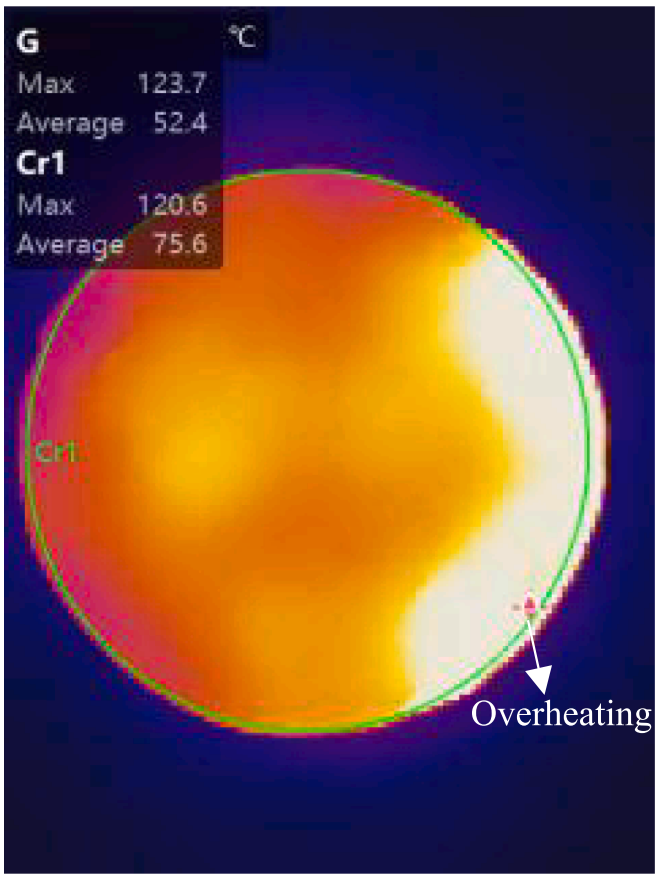

Fig. 18. The thermal image of the asphalt mixture heating up and the test results of the average temperature of the asphalt mixture surface.

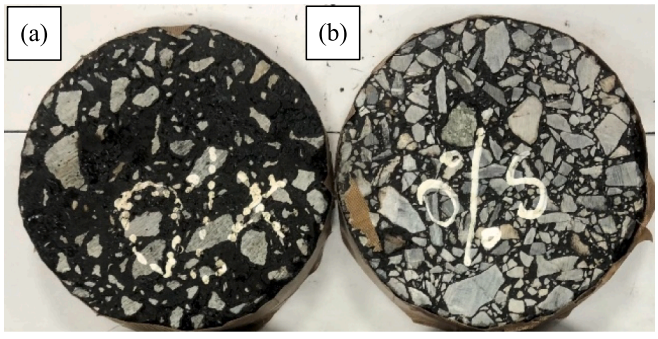

Fig. 19. Surface morphology of the specimens under multiple microwave irradiation (a. 07BL; b. 07L).

3.3.2. 25 °C fatigue test results

Fig. 24 shows the results of repeated fatigue test results for asphalt mixtures at 25 °C. The H_{na} was 25.4% for 7BL and 5.2% for 7L, and the self-healing effect of 7BL under the action of the microwave was 4.88 times that of 7L. The H_{na} of asphalt mixture containing basalt was significantly higher than that of asphalt mixture containing only limestone. Compared with the SCB test at −10 °C, the healing effect of the fatigue test at 25 °C was poor. For specimens containing basalt, the microwave healing effect after 25 °C fatigue was 30%–50% of that after −10 °C fracture. For limestone specimens, the microwave healing effect after 25 °C fatigue was within 20% of that after −10 °C fracture. Because the structural deformation of the specimens was larger in the process of fatigue, and the destroy gap of the specimens after fatigue was larger, so the destroyed surface of the specimens after destroy can't be well-matched, while the destroyed surface of the specimens under −10 °C fracture was well matched. Therefore, the microwave self-healing effect of the asphalt mixture after fatigue was poor.

4. Conclusions

The basalt and limestone composite grading methods were used to prepare the asphalt mixture with better wave-absorbing ability, and the microwave heating self-healing rate was proposed to be improved by increasing the microwave loss of the asphalt mixture. The microwave heating mechanism of basalt was revealed through the physicochemical and electromagnetic properties of basalt. It was verified that basalt can improve the self-healing rate of asphalt mixture through heating temperature test and microwave self-healing test of asphalt mixture.

(1) In basalt, Si and its oxides account for the largest proportion, and the remaining top 7 elements or oxides are all metal elements and metal oxides. Due to the oxidation of air, the Fe^{2+} content in the basalt decreases continuously, and the microwave loss ability was weakened. The main phases of basalt were the combination of Si and ferrite, or the combination of Si and metal Fe and Al, indicating that basalt can absorb waves. In the microwave frequency range of 1–18 GHz, due to the $Tan\delta_M$ of basalt was slightly larger than $Tan\delta_E$, it had the characteristics of both dielectric loss and magnetic loss, but mainly generates heat through magnetic loss.
(2) Different types of aggregates had different heating effects under the action of microwaves, basalt had a higher heating rate than limestone. Due to the different particle sizes of basalt, its microwave heating effect was also different, basalt with small particle sizes has a better heating rate.
(3) The microwave heating results of the asphalt mixture show that the heating rate curves of the two asphalt mixtures show a non-complete linear relationship. The heating rate of the asphalt mixture with basalt and limestone aggregates specimens was 1.44 times that of the limestone asphalt mixture.
(4) The results of the −10 °C SCB test showed that the fracture energy and the maximum axial force at fracture of the healed asphalt mixture did not increase or decreased with the increase of the healing times. When the specimens healed under the action of microwave, the temperature at the crack was higher. In terms of the H_{ea} and H_{fa}, the microwave self-healing effect of 7BL was about 2.50 times that of 7L. The fatigue test results showed that the microwave self-healing effect of 7BL was 4.88 times that of 7L. The flexural strength and fatigue resistance of asphalt mixture with basalt and limestone aggregates can be restored by at least 65% and 23% respectively after microwave healing.

Through this study, after repeated microwave heating of the asphalt mixture with basalt and limestone aggregates, it can still maintain a high self-healing rate, and the flexural strength and fatigue resistance can recover at least 65% and 23% respectively. The recommended microwave heating time is 2 min, which can make the temperature of the asphalt mixture reach about 120 °C. The asphalt mixture with basalt and limestone aggregates can be used in the road sections with high traffic flow and prone to road distresses in the future. On the one hand, it can reduce the traffic problems caused by maintenance, and on the other hand, it can restore the road performance to a better level.

Funding

The authors acknowledge the Transportation Technology Project of Department of Transport of Hubei Province (No. 2022-11-1-10), the financial supported by the National Key R&D Program of China (No. 2018YFB1600200), the Plan of Outstanding Young and Middle-aged Scientific and Technological Innovation Team in Universities of Hubei Province (No. T2020010), the scientific research fund project of Wuhan

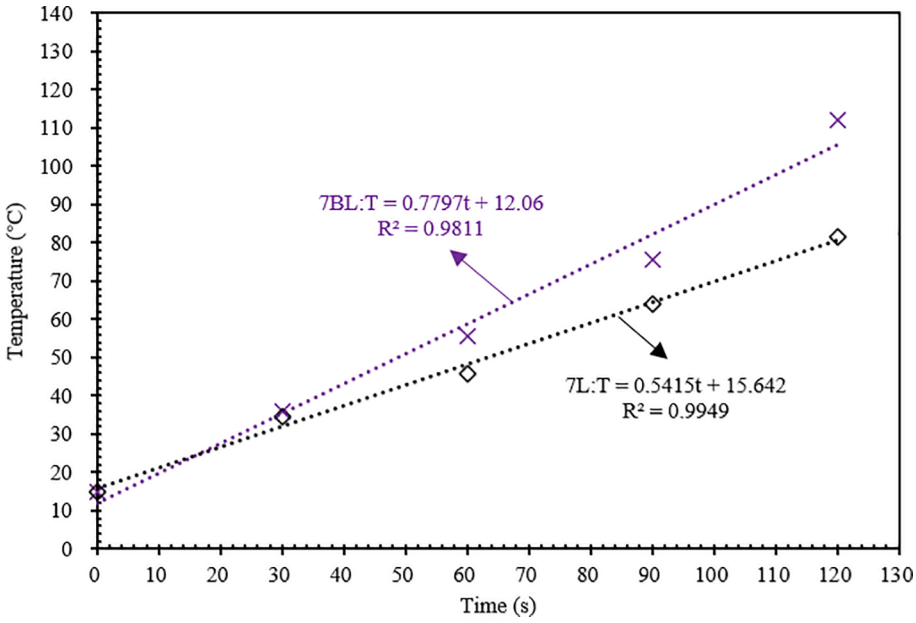

Fig. 20. Results of microwave heating of asphalt mixtures for 0–120 s.

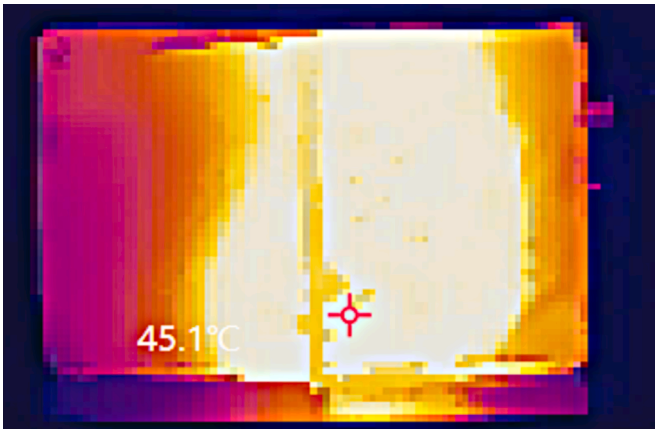

Fig. 21. Thermal image of the specimen after microwave heating.

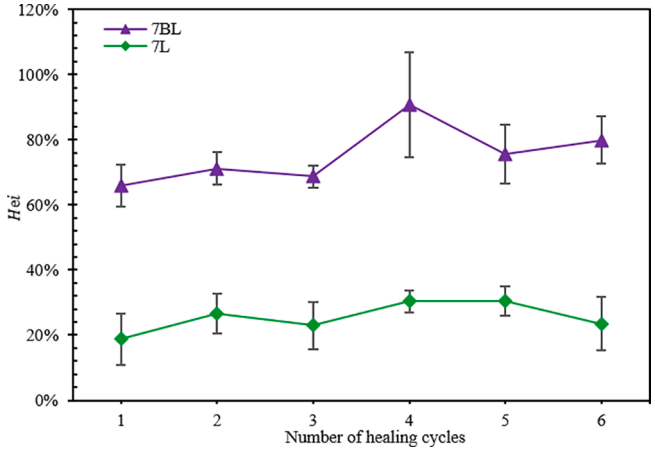

Fig. 22. The relationship between the number of healing cycles and H_{ei}.

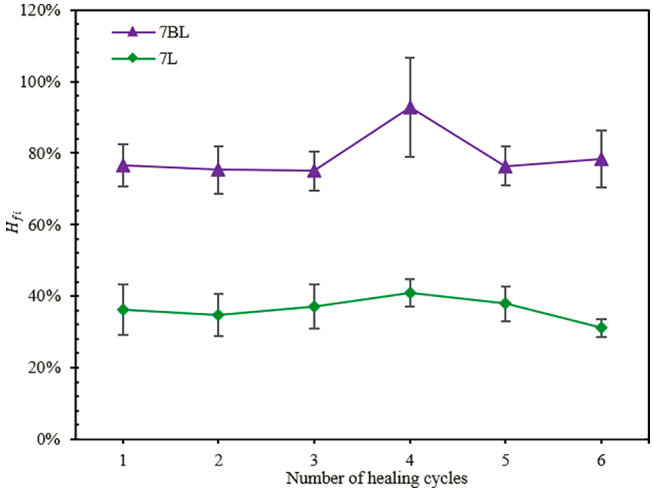

Fig. 23. The relationship between the number of healing cycles and H_{fi}.

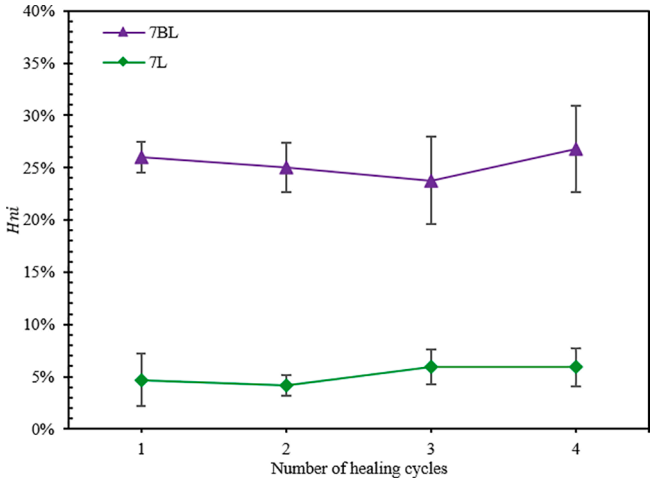

Fig. 24. The relationship between the number of healing cycles and H_{ni}.

Institute of Technology (No. K2021032), European Union's Horizon 2020 Research and Innovation Programme under the Marie Skłodowska-Curie grant agreement (No. 101030767), and the test help from Shiyanjia Lab (www.shiyanjia.com).

CRediT authorship contribution statement

Fu Wang: Methodology, Data curation, Writing – original draft. **Hongbin Zhu:** Data curation, Writing – original draft, Validation. **Benan Shu:** Methodology, Data curation. **Yuanyuan Li:** Conceptualization, Methodology, Data curation, Writing – original draft, Writing – review & editing, Supervision, Funding acquisition. **Dengjun Gu:** Methodology, Project administration. **Yangming Gao:** Methodology, Writing – review & editing. **Anqi Chen:** Resources, Software, Writing – review & editing. **Jianlin Feng:** Resources, Data curation, Software, Validation. **Shaopeng Wu:** Methodology, Validation, Funding acquisition. **Quantao Liu:** Data curation, Software. **Chao Li:** Methodology, Writing – review & editing.

Declaration of Competing Interest

The authors declare that they have no known competing financial interests or personal relationships that could have appeared to influence the work reported in this paper.

References

[1] A. Bhasin, D.N. Little, R. Bommavaram, K. Vasconcelos, A framework to quantify the effect of healing in bituminous materials using material properties, Road Mater. Pavement Design 9 (sup1) (2008) 219–242.
[2] B. Lou, A. Sha, Y. Li, W. Wang, Z. Liu, W. Jiang, X. Cui, Effect of metallic-waste aggregates on microwave self-healing performances of asphalt mixtures, Constr. Build. Mater. 246 (2020) 118510.
[3] P. Cui, S. Wu, Y. Xiao, R. Hu, T. Yang, Environmental performance and functional analysis of chip seals with recycled basic oxygen furnace slag as aggregate, J. Hazard. Mater. 405 (2021) 124441.
[4] Y. Li, J. Feng, F. Yang, S. Wu, Q. Liu, T. bai, Z. Liu, C. Li, D. Gu, A. Chen, Y. Jin, Gradient aging behaviors of asphalt aged by ultraviolet lights with various intensities, Constr. Build. Mater. 295 (2021) 123618.
[5] N. Ruiz-Riancho, A. Garcia, D. Grossegger, T. Saadoon, R. Hudson-Griffiths, Properties of Ca-alginate capsules to maximise asphalt self-healing properties, Constr. Build. Mater. 284 (2021) 122728.
[6] L. Trigos, J.I. Escavy, J. Gallego, F. Gulisano, Natural factors related to the differential heating of aggregates exposed to microwaves, Constr. Build. Mater. 314 (2022) 125654.
[7] H.M.Z. Hassan, K. Wu, W. Huang, S. Chen, Q. Zhang, J. Xie, X.u. Cai, Study on the influence of aggregate strength and shape on the performance of asphalt mixture, Constr. Build. Mater. 294 (2021) 123599.
[8] G. Xu, J. Fan, T. Ma, W. Zhao, X. Ding, Z. Wang, Research on application feasibility of limestone in sublayer of Double-Layer permeable asphalt pavement, Constr. Build. Mater. 287 (2021) 123051.
[9] F. Tao, J. Wen, O. Hua, Road performance of mixed diabase aggregate and limestone aggregate, Transp. Res. (2015).
[10] D.D. Guo, Study on water stability of granite asphalt mixture, Adv. Mater. Res. 724–725 (2013) 1555–1559.
[11] W. Jiao, A. Sha, Z. Liu, W. Jiang, L. Hu, X. Li, Utilization of steel slags to produce thermal conductive asphalt concretes for snow melting pavements, J. Cleaner Prod. 261 (2020), 121197.
[12] G.G. Al-Khateeb, T.S. Khedaywi, T.-S. Obaidat, A.M. Najib, Laboratory study for comparing rutting performance of limestone and basalt superpave asphalt mixtures, J. Mater. Civ. Eng. 25 (1) (2013) 21–29.
[13] W. Xu, Y.I. Shah, D. Luan, S. Tian, Evaluation of moisture damage of cold patch asphalt using the surface free energy method, Civil Eng. 46 (11) (2021) 11267–11277.
[14] J. Zhu, K. Zhang, K. Liu, X. Shi, Adhesion characteristics of graphene oxide modified asphalt unveiled by surface free energy and AFM-scanned micro-morphology, Constr. Build. Mater. 244 (2020) 118404.
[15] Y. Gao, Y. Zhang, F. Gu, T. Xu, H. Wang, Impact of minerals and water on bitumen-mineral adhesion and debonding behaviours using molecular dynamics simulations, Constr. Build. Mater. 171 (2018) 214–222.
[16] Y. Gao, Y. Zhang, Y. Yang, J. Zhang, F. Gu, Molecular dynamics investigation of interfacial adhesion between oxidised bitumen and mineral surfaces, Appl. Surf. Sci. 479 (2019) 449–462.
[17] R.P. Panda, S.S. Das, P.K. Sahoo, Optimum bitumen content for bituminious concrete – an alternative approach for estimation, Int. J. Civil Eng. Technol. 8 (810) (2017) 435–453.
[18] J. Ji, Y. Dong, R. Zhang, Z. Suo, C. Guo, X.u. Yang, Z. You, Effect of water absorption and loss characteristics of fine aggregates on aggregate-asphalt adhesion, KSCE J. Civ. Eng. 25 (6) (2021) 2020–2035.
[19] S. Prasad, H. Chouhan, K. Kartikeya, K.K. Singh, N. Bhatnagar, An Experimental Investigation into Mechanical behaviour of Basalt PEI laminates at various strain rates, Compos. Struct. 267 (2021) 113800.
[20] J. Li, J. Yu, S. Wu, J. Xie, The mechanical resistance of asphalt mixture with steel slag to deformation and skid degradation based on laboratory accelerated heavy loading test, Materials 15 (3) (2022) 911.
[21] B. Liang, F. Lan, K. Shi, G. Qian, Z. Liu, J. Zheng, Review on the self-healing of asphalt materials: Mechanism, affecting factors, assessments and improvements, Constr. Build. Mater. 266 (2021) 120453.
[22] P. Wan, Q. Liu, S. Wu, Z. Zhao, S. Chen, Y. Zou, W. Rao, X. Yu, A novel microwave induced oil release pattern of calcium alginate/nano-Fe3O4 composite capsules for asphalt self-healing, J. Cleaner Prod. 297 (2021) 126721.
[23] J.L. Concha, J. Norambuena-Contreras, Thermophysical properties and heating performance of self-healing asphalt mixture with fibres and its application as a solar collector, Appl. Therm. Eng. 178 (2020) 115632.
[24] E. Yalcin, Effects of microwave and induction heating on the mechanical and self-healing characteristics of the asphalt mixtures containing waste metal, Constr. Build. Mater. 286 (2021) 122965.
[25] M.T. Bevacqua, T. Isernia, F.G. Praticò, S. Zumbo, A method for bottom-up cracks healing via selective and deep microwave heating, Autom. Constr. 121 (2021) 103426.
[26] Z. Peng, J. Yang, Microwave-assisted metallurgy, Int. Mater. Rev. 60 (1) (2014) 30–63.
[27] C. Guo, W. Zhang, R. Wang, S. Qi, Enhanced electromagnetic wave absorption by optimized impedance matching: covalently bonded polyaniline nanorods over graphene nanoplates, J. Mater. Sci. Mater. Electron. 30 (21) (2019) 19426–19436.
[28] S. Goel, A. Garg, H.B. Baskey, S. Tyagi, Microwave absorption study of low-density composites of barium hexaferrite and carbon black in X-band, J. Sol-Gel Sci. Technol. 98 (2) (2021) 351–363.
[29] T. Luo, L. Xu, J. Peng, L. Zhang, Y.i. Xia, S. Ju, J. Liu, R. Gang, Z. Wang, Efficient preparation of Si3N4 by microwave treatment of solar-grade waste silicon powder, ACS Omega 5 (11) (2020) 5834–5843.
[30] M.A. Aslam, K. Hu, W. Ding, A. Hassan, Y. Bian, K. Qiu, Qiangchun liu, Z. Sheng, Dimensionality determined microwave absorption properties in ferrite/bio-carbon composites, Ceram. Int. 47 (19) (2021) 27496–27502.
[31] L. Trigos, J. Gallego, J.I. Escavy, L. Picado-Santos, Dielectric properties versus microwave heating susceptibility of aggregates for self-healing asphalt mixtures, Constr. Build. Mater. 293 (2021) 123475.
[32] W. Yang, B. Jiang, S. Che, L. Yan, Z.-X. Li, Y.-F. Li, Research progress on carbon-based materials for electromagnetic wave absorption and the related mechanisms, New Carbon Mater. 36 (6) (2021) 1016–1030.
[33] H. Wang, Y. Zhang, Y.i. Zhang, S. Feng, G. Lu, L. Cao, Laboratory and numerical investigation of microwave heating properties of asphalt mixture, Materials 12 (1) (2019) 146.
[34] Z. Jun, F. Huiqing, W. Yangli, Z. Shiquan, X. Jun, C. Xinying, Ferromagnetic and microwave absorption properties of copper oxide/cobalt/carbon fiber multilayer film composites, Thin Solid Films 520 (15) (2012) 5053–5059.
[35] Z. Wang, P. Zhao, T. Ai, G. Yang, Q. Wang, Microwave absorbing characteristics of asphalt mixes with carbonyl iron powder, Progr. Electromagn. Res. 19 (2011) 197–208.
[36] Fernández González Antonio, Propiedades dielétricas de los materiales del sector metalúrgico para su posterior aplicación en microondas, Trabajos académicos (2014).
[37] J. Kuang, P. Jiang, F. Ran, W. Cao, Conductivity-dependent dielectric properties and microwave absorption of Al-doped SiC whiskers, J. Alloy. Compd. 687 (2016) 227–231.
[38] Y. Shi, L. Yu, K. Li, S. Li, Y. Dong, Y. Zhu, Y. Fu, F. Meng, Well-matched impedance of polypyrrole-loaded cotton non-woven fabric/polydimethylsiloxane composite for extraordinary microwave absorption, Compos. Sci. Technol. 197 (2020) 108246.
[39] W. Huang, L. Peng, H. Ming. Comparison of the Fatigue Performance of Asphalt Mixtures Considering Self-Healing, in: Proceedings of the 2015 International Symposium on Frontiers of Road and Airport Engineering, F, 2015.
[40] J. Yang, H. Wang, L. Hui, et al., Key influential factors of fatigue and self-healing properties of asphalt mixture, J. Southeast Univ. (Nat. Sci. Ed.) (2016).
[41] M. Atakan, K. Yildiz. Self-healing potential of porous asphalt concrete containing different aggregates and metal wastes through microwave heating. 2021.
[42] China Ministry of Transport of the People's Republic of. Standard test methods of bitumen and bituminous mixtures for highway engineering: JTG E20-2011. Beijing: China Communications Press, 2011.
[43] Communications Highway Research Institute of the Ministry of. Technical Specifications for Construction of Highway Asphalt Pavements: JTG F40-2004. Beijing: China Communications Press, 2009.
[44] Institute of Highway Science Ministry of Communications. Test Methods of Aggregate for Highoay Engineering: JTG E42-2005. Beijing: People's Communications Press, 2005.
[45] J. Li, B. Li, B. Zhang, et al. Microwave carbothermic reduction from Fe_2O_3 to Fe_3O_4 powders. J. Univ. Sci. Technol. Beijing, 2011.
[46] H. Guo, Z. Wang, J. Huo, X. Wang, Z. Liu, G. Li, Microwave heating improvement of asphalt mixtures through optimizing layer thickness of magnetite and limestone aggregates, J. Cleaner Prod. 273 (2020) 123090.

[47] W. Xu, Z. Yin, J. Yuan, Z. Wang, Y. Fang, Effects of sintering additives on mechanical properties and microstructure of Si 3 N 4 ceramics by microwave sintering, Mater. Sci. Eng., A 684 (2017) 127–134.
[48] K. Singh, A.V. Nirmal, S.V. Sharma, Study the loss of microstrip on silicon, Microwaves Rf (2017).
[49] S.H. Hosseini, S.H. Mohseni, A. Asadnia, H. Kerdari, Synthesis and microwave absorbing properties of polyaniline/$MnFe_2O_4$ nanocomposite, J. Alloys Compds. 509 (14) (2011) 4682–4687.
[50] Y. Gao, Y. Zhao, Q. Jiao, et al., Microemulsion-based synthesis of porous Co-Ni ferrit nanorods and their magnetic properties, J. Alloy. Compd. 555 (2013) 95–100.
[51] Z. Luo, X. Fan, B. Feng, et al. Highly enhancing electromagnetic properties in Fe-Si/MnO-SiO 2 soft magnetic composites by improving coating uniformity. 2021.
[52] Y. Janu, D. Chaudhary, V. Chauhan, et al., Preparation of Fe–Si–Al intermetallic alloy and their composite coating for EM absorbing application in 6–18 GHz. SN, Appl. Sci. 2 (5) (2020).
[53] N.a. Gao, W.-P. Li, W.-S. Wang, D.-P. Liu, Y.-M. Cui, L. Guo, G.-S. Wang, Balancing dielectric loss and magnetic loss in Fe-NiS2/NiS/PVDF composites toward strong microwave reflection loss, ACS Appl. Mater. Interfaces 12 (12) (2020) 14416–14424.
[54] S. Zhu, J. Shi, T. Sun, Application of microwave methods to asphalt pavements maintenance, Mater. Rev. (2007).
[55] H. Zhu, H. Yuan, Y. Liu, S. Fan, Y. Ding, Evaluation of self-healing performance of asphalt concrete for macrocracks via microwave heating, J. Mater. Civ. Eng. 32 (9) (2020) 04020248.